ISSN 1070-3284, Russian Journal of Coordination Chemistry, 2024, Vol. 50, No. 7, pp. 427–439. © Pleiades Publishing, Ltd., 2024.

Complexes of Hexacoordinated Ni(II) Based on Diacetyl Bis-hetarylhydrazones: Structures and Magnetic Properties

M. V. Melikhov[a], D. V. Korchagin[b,] *, Yu. P. Tupolova[a,] **, L. D. Popov[a], V. A. Chetverikova[a], V. V. Tkachev[b], A. N. Utenyshev[b], N. N. Efimov[c], I. N. Shcherbakov[a], and S. M. Aldoshin[b]

[a] *Southern Federal University, Rostov-on-Don, Russia*

[b] *Federal Research Center of Problems of Chemical Physics and Medicinal Chemistry, Russian Academy of Sciences, Chernogolovka, Moscow oblast, Russia*

[c] *Kurnakov Institute of General and Inorganic Chemistry, Russian Academy of Sciences, Moscow, Russia*

**e-mail: korden@icp.ac.ru*

***e-mail: yptupolova@sfedu.ru*

Received February 5, 2024; revised February 21, 2024; accepted March 13, 2024

Abstract—Mononuclear nickel complexes $[NiL^1(NCS)_2]\cdot 2DMSO$ (**I**), $[NiL^1(NCS)_2]\cdot DMF$ (**II**), and $[NiL^2(NCS)_2]\cdot 0.5CH_3OH\cdot 1.5H_2O$ (**III**) with the distorted octahedral coordination node, where L^1 and L^2 are the tetradentate ligand systems derived from the products of the condensation of diacetyl with 2-hydrazinoquinoline and 2-hydrazino-4,6-dimethylpyrimidine, respectively, are synthesized. The structures of the compounds are determined by IR spectroscopy and XRD (CIF files CCDC nos. 2219793 (**I**), 2142035 (**II**), and 2219794 (**III**)). The quantum chemical modeling of the axial parameter of magnetic anisotropy in the zero field (*D*) is performed for the synthesized compounds in the framework of the SA-CASSCF+NEVPT2 method. The complexes are shown to be characterized by three-axis magnetic anisotropy close to the light magnetization plane with positive *D*. The axial parameter of magnetic anisotropy ($D_{exp} = 8.79$ cm^{-1}) determined by the approximation of the magnetometry data on complex $[NiL^2(NCS)_2]\cdot 0.5CH_3OH\cdot 1.5H_2O$ is consistent with the calculated value ($D_{calc} = 11.5$ cm^{-1}).

Keywords: bis-hetarylhydrazones, nickel(II) complexes, quantum chemical modeling, axial parameter of magnetic anisotropy, XRD

DOI: 10.1134/S1070328424600396

INTRODUCTION

Research in the area of monomolecular magnetism is one of the most urgent trends of the modern coordination chemistry. Increased interest in single molecule magnets (SMM) is due to prospects of their use in superdense data storage and processing devices and in the field of spintronics and quantum calculations [1–5]. It is known that the ability of compounds to exhibit the properties of SMM, i.e., to retain magnetization within one molecule for a prolonged time, depends on the presence of an energy barrier between two opposite orientations of the magnetic moment, the value of which is primarily predetermined by the axial parameter of magnetic anisotropy (*D*) [6–9]. Therefore, the study of factors affecting the sign and value of *D* is important for the target synthesis of molecular magnetic materials. Among these factors are the structure of the coordination polyhedron, nature of the ligands and complexing metal, crystal packing of the complexes, etc. [10–14]. Mononuclear complexes of 3*d* metals are used as models for studying the influence of the molecular structure of compounds on *D*. This is due to the fact that the purposeful choice of the ligand system makes it possible to prepare metal chelates with a certain symmetry of the coordination polyhedron and the ligand field strength, which affects, in turn, the splitting of *d*-AO, spin state of the system, and, as a consequence, the axial parameter of magnetic anisotropy. Many mononuclear Co(II) and Fe(II) complexes characterized by high *D* and exhibiting the properties of single-ion magnets (SIM) are known [10–12].

One of the promising classes of polydentate ligand systems used for the synthesis of coordination compounds includes hydrazones and azomethines of dicarbonyl compounds [15, 16]. We have previously synthesized the hexacoordinated Co(II) complexes of bis-hydrazones, which are the products of diacetyl condensation with 2-hydrazinoquinoline and 2-hydrazino-4,6-dimethylpyrimidine, demonstrating the field-induced behavior of SIM [17–19]. The targeted choice of these bis-hydrazones as ligand systems was due to their rigid tetradentate N_4-donor structure that favored the distortion of the coordination mode

toward trigonal prismatic symmetry. It is the closeness of the coordination polyhedron structure of a trigonal prism which predetermines strong magnetic anisotropy of the axial type and properties of SIM in the Co(II) complexes. Continuing these studies, we synthesized and structurally characterized the nickel(II) complexes $[NiL^1(NCS)_2]\cdot 2DMSO$ (**I**), $[NiL^1(NCS)_2]\cdot DMF$ (**II**), and $[NiL^2(NCS)_2]\cdot 0.5CH_3OH\cdot 1.5H_2O$ (**III**), where L^1 and L^2 are diacetyl bis-quinolyl- and bis-dimethylpyrimidylhydrazones, respectively. The splitting parameters in the zero field (components of the *g* and *D* tensor) of the synthesized complexes were calculated by quantum-chemical modeling, and their electronic and geometric structures were studied.

EXPERIMENTAL

2-Hydrazinoquinoline and 2-hydrazino-4,6-dimethylpyrimidine were synthesized according to previously described procedures [20, 21]. Diacetyl bis-quinolylhydrazone (L^1) [22] and diacetyl bis-dimethylpyrimidylhydrazone (L^2) [19] were synthesized according to known procedures. All other reagents and solvents were purchased from commercial sources and used as received. The IR spectra of solid samples were recorded on a Varian Scimitar 1000 FT-IR spectrometer in a range of 400–4000 cm^{-1}. Elemental analyses to C, H, and N were carried out on a PerkinElmer 240C instrument. The nickel content was determined by gravimetry after a sample of the complex was calcined in air access to a constant weight.

Synthesis of $[NiL^1(NCS)_2]\cdot 2DMSO$ (I) and $[NiL^1(NCS)_2]\cdot DMF$ (II). A hot solution of $Ni(ClO_4)_2\cdot 6H_2O$ (0.146 g, 0.4 mmol) in methanol (6 mL) was poured to a boiling solution of L^1 (0.15 g, 0.4 mmol) in methanol (7 mL), and the solution turned brown. After 5 min, solid KSCN (0.079 g, 0.8 mmol) was added, and an amorphous brown precipitate was formed. The reaction mixture was refluxed for 3 h. The precipitate was filtered off and washed with methanol.

Dark green crystals of $[NiL^1(NCS)_2]\cdot 2DMSO$ (**I**) were formed in several days due to the recrystallization of the formed precipitate from DMSO. The yield was 0.19 g (68%). $T_m > 260$°C.

For $C_{28}H_{32}N_8O_2S_4Ni$

Anal. calcd., %	C, 48.07	H, 4.61	N, 16.02	Ni, 8.39	O, 4.57; S, 18.33
Found, %	C, 47.9	H, 4.7	N, 16.1	Ni, 8.2	

IR (ν, cm^{-1}): 3132 m (NH), 2096 s (NCS^-), 1633 m (C=N), 1618 m (C=N), 1602 s (C=N), 1579 m, 1521 s, 1483 m, 1424 m, 1384 w, 1322 m, 1312 m, 1257 w, 1241 s, 1229 s, 1178 m, 1116 m, 971 m, 943 m, 864 w, 815 s, 774 m, 749 s, 624 s, 553 m, 529 m, 512 m, 485 w, 469 w, 448 w, 423 w.

Dark green crystals of $[NiL^1(NCS)_2]\cdot DMF$ (**II**) were formed in several days due to recrystallization from DMF. The yield was 0.16 g (64%). $T_m > 260$°C.

For $C_{27}H_{27}N_9OS_2Ni$

Anal. calcd., %	C, 52.61	H, 4.41	N, 20.45	Ni, 9.52	O, 2.60	S, 10.40
Found, %	C, 52.7	H, 4.3	N, 20.6	Ni, 9.3		

IR (ν, cm^{-1}): 3191 (NH), 3139 m (NH), 2093 s (NCS^-), 2049 s (NCS^-), 1664 s (C=N), 1605 s (C=N), 1569 s (C=N), 1520 m, 1477 m, 1426 m, 1388 w, 1310 m, 1239 w, 1185 m, 1146 m, 1105 m, 978 w, 953 m, 819 s, 775 s, 750 s, 668 m, 634 m, 578 w, 515 w, 475 w, 444 w.

Synthesis of $[NiL^2(NCS)_2]\cdot 0.5CH_3OH\cdot 1.5H_2O$ (III). A hot solution of $Ni(ClO_4)_2\cdot 6H_2O$ (0.17 g, 0.46 mmol) in methanol (3 mL) was poured to a boiling solution of L^2 (0.15 g, 0.46 mmol) in methanol (5 mL), and the solution turned brown. After 5 min, solid KSCN (0.09 g, 0.92 mmol) was added, and a green crystalline precipitate was formed. The reaction mixture was refluxed for 3 h. The precipitate was filtered off and recrystallized from a DMSO–methanol mixture. After 3 days, green crystals of complex **III** were formed in the solution. The yield was 0.15 g (61%). $T_m > 260$°C.

For $C_{18.5}H_{27}N_{10}O_2S_2Ni$

Anal. calcd., %	C, 40.82	H, 5.00	N, 25.73	Ni, 10.78	O, 5.88	S, 11.78
Found, %	C, 40.3	H, 5.0	N, 25.9	Ni, 10.8		

IR (ν, cm^{-1}): 3563, 3382 m (OH, solvent), 3159 m (NH), 2104, 2062 s (NCS^-), 1631 m (C=N), 1602 m (C=N), 1555 s, 1433 s, 1387 m, 1364 s, 1347 m, 1329 s, 1248 m, 1229 w, 1207 m, 1187 m, 1132 m, 1031 w, 998 w, 847 m, 810 w, 785 w, 692 w, 627 m, 538 m, 520 w, 490 w, 486 w.

Magnetic data were obtained on a Quantum Design PPMS-9 system for measuring physical properties (Quantum Design). The temperature dependence of the magnetic susceptibility of compound **III** was measured for a polycrystalline sample in a temperature range of 2–300 K in an applied magnetic field of 0.5 T. The diamagnetic correction was calculated by Pascal's scheme. The field dependence of the magnetization of the sample was measured at T = 1.8 and 5 K.

XRD of single-crystal samples of compounds **I**–**III** was conducted on an XCalibur automated diffractometer (Agilent) with an EOS CCD coordinate detector (Agilent Technologies UK Ltd., Yarnton, Oxfordshire, England). Reflections were collected and unit cell parameters were determined and refined using the specialized CrysAlis PRO software [23]. The XRD data were obtained at the temperature of the samples 100.0(1) K using MoK_α radiation (λ = 0.71073 Å). The

Table 1. Crystallographic data and experimental structure refinement parameters for compounds **I**–**III**

Parameter	Value		
	I	**II**	**III**
Empirical formula	$C_{24}H_{20}N_8S_2Ni{\cdot}2(C_2H_6OS)$	$C_{24}H_{20}N_8S_2Ni{\cdot}C_3H_7NO$	$C_{18}H_{22}N_{10}S_2Ni{\cdot}0.5(CH_4O){\cdot}1.5(H_2O)$
T, K	100	100	100
Crystal system	Monoclinic	Triclinic	Monoclinic
Space group	$C2/c$	$P\bar{1}$	$P2_1/n$
a, Å	14.5773(9)	9.7429(5)	11.5401(10)
b, Å	13.9580(6)	10.5293(5)	15.7363(11)
c, Å	17.1312(9)	14.0584(7)	13.7381(10)
α, deg	90	96.241(4)	90
β, deg	113.833(6)	103.499(4)	100.391(9)
γ, deg	90	98.247(4)	90
V, Å^3	3188.5(3)	1372.62(12)	2453.903
Z	4	2	4
ρ_{calc}, g cm^{-3}	1.457	1.491	1.465
μ, mm^{-1}	0.911	0.899	0.998
F(000)	1456	640	1124
Range of θ, deg	2.8, 26.3	2.9, 29.1	3.0, 29.1
Range of indices hkl	$-18 \le h \le 18$, $-15 \le k \le 17$, $-21 \le l \le 20$	$-13 \le h \le 13$, $-14 \le k \le 14$, $-17 \le l \le 19$	$-15 \le h \le 15$, $-21 \le k \le 10$, $-18 \le l \le 10$
Number of reflections measured/independent	7093, 3252	12 694, 7328	12 690, 6562
Completeness to θ = max	0.998	0.995	0.999
Number of parameters	236	361	324
R_1, wR_2 ($I > 2\sigma(I)$)	0.0347, 0.0769	0.0361, 0.0765	0.0520, 0.1106
R_1, wR_2 (all data)	0.0422, 0.0804	0.0486, 0.0826	0.0815, 0.1205
$\Delta\rho_{min}/\Delta\rho_{max}$, e/Å^3	−0.33/0.41	−0.38/0.36	−0.90/0.67

structures were solved by direct methods. The full-matrix refinement of the positions and thermal parameters of non-hydrogen atoms was isotropic and then anisotropic using least squares. All calculations were performed using the SHELXTL program package [24]. In the structure of compound **I**, the DMSO molecule is disordered over two positions. The crystals of compound **III** contain the coordination compound $[NiL^2(NCS)_2]$ and additionally two molecules of water of crystallization bearing the O(1) and O(2*w*) oxygen atoms. One of these molecules (with the O(2*w*) atom) is statistically uniformly substituted by the methanol molecule, and hydrogen atoms for this molecule were not determined. Selected crystallographic characteristics of compounds **I**–**III** are given in Table 1.

The full structural information for compounds structures **I**–**III**, including the distances and angles in the molecules, was deposited with the Cambridge Crystallographic Data Centre (CIF files CCDC nos. 2219793 (**I**), 2142035 (**II**), and 2219794 (**III**); www.ccdc.cam.ac.uk/data_request/cif).

The electronic structures of the complexes were calculated in the framework of the multiconfigurational method of state-average complete active space self-consistent field (SA-CASSCF) [25–27] followed by refinement in the framework of the second-order n-electron valence state perturbation theory

(NEVPT2) [28–31]. Scalar relativistic effects were taken into account in the Douglas–Kroll–Hess approximation [32]. The segmented all-electron relativistically contracted (SARC) variant [33] of the three-exponent Ahlrichs basis set extended by polarization functions of the def2-TZVP type was used for all atoms [33–36]. The electron density expansion in the auxiliary basis set was used to reduce the calculation time [37]. Spin-orbital interaction was taken into account in terms of the quasi-degenerate perturbation theory (QDPT) [8]. All calculations were performed using the ORCA v. 4.1.1 program [38].

Five molecular orbitals (MO) with the predominant contribution of the 3*d*-AOs of the nickel atom and eight electrons corresponding to the d^8 electron configuration were included into the CAS(8,5) active space. All possible multiplet states were included into the wavefunction expansion.

The coordinates of non-hydrogen atom nuclei were taken from the XRD results, and the positions of hydrogen atoms were preliminarily optimized using the BP86 functional and def2-TZVP basis set.

The *d*-orbital splitting was analyzed by the ab initio ligand field theory (AILFT) [39, 40] implemented in the ORCA program. The *D* and *g* tensors were calculated in terms of the effective Hamiltonian approximation.

RESULTS AND DISCUSSION

Bis-hetarylhydrazones L^1 and L^2 and their Ni(II) complexes, $[NiL^1(NCS)_2]\cdot 2DMSO$ (**I**), $[NiL^1(NCS)_2]\cdot DMF$ (**II**), and $[NiL^2(NCS)_2]\cdot 0.5CH_3OH\cdot 1.5H_2O$ (**III**), were synthesized according to Schemes 1 and 2.

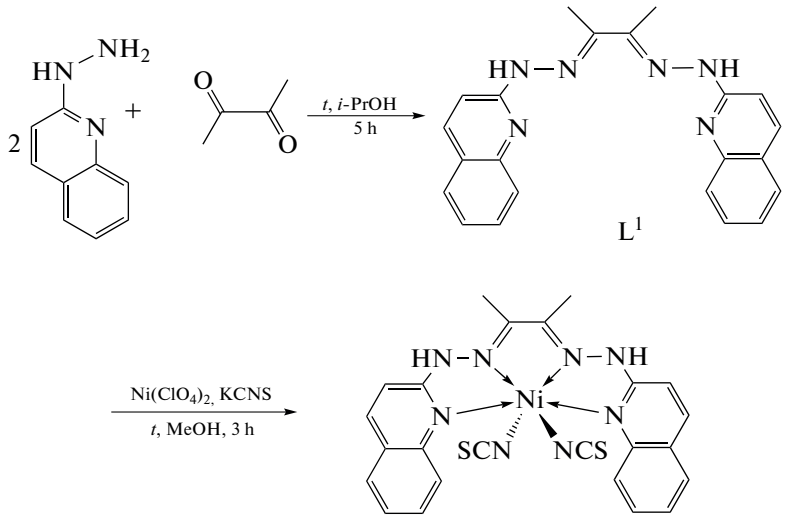

Scheme 1.

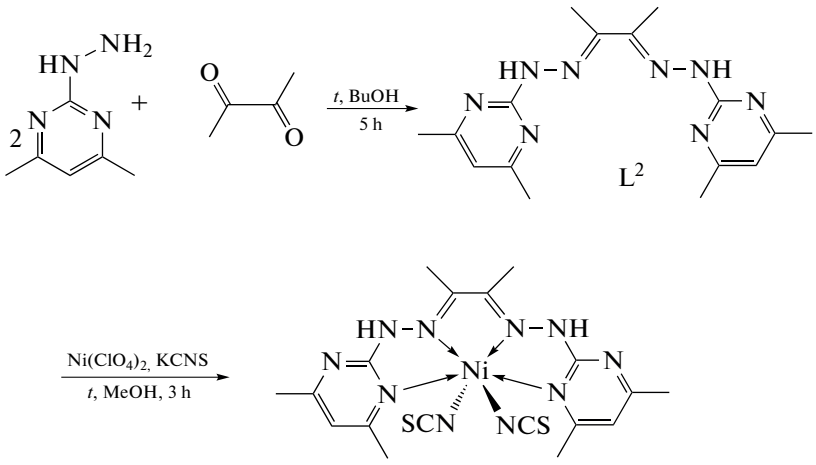

Scheme 2.

The compositions and structures of complexes **I**–**III** were determined by elemental analysis, IR spectroscopy, and XRD.

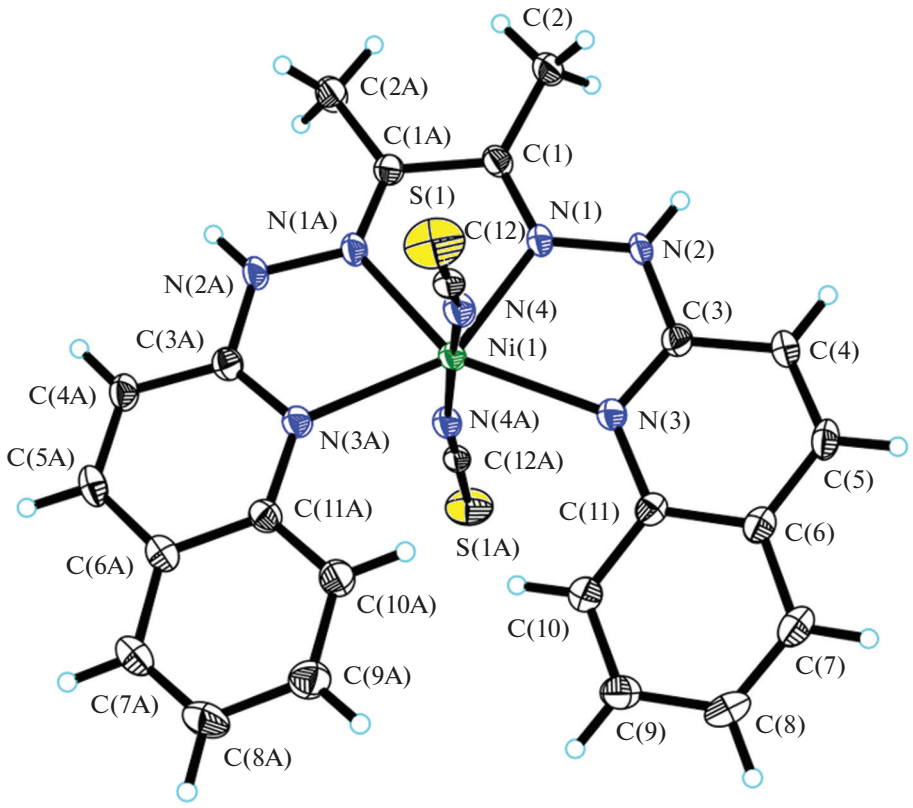

Fig. 1. Molecular structure of complex **I** (without DMSO molecule).

The IR spectra of the complexes in a range of 3191–3132 cm^{-1} exhibit the absorption band corresponding to stretching vibrations of the NH groups. The absorption bands of stretching vibrations of the C=N groups experience shifts by 15–40 cm^{-1} compared to the spectrum of the ligand and are observed as high- and medium-intensity bands in a range of 1634–1569 cm^{-1}. The data obtained indicate that bishydrazones L^1 and L^2 in complexes **I**–**III** behave as tetradentate ligand systems in the neutral form coordinating to the nickel ion by the nitrogen atoms of the azomethine and heterocyclic fragments. The presence of NCS anions in the complexes is confirmed by the high-intensity absorption band in a range of 2104–2049 cm^{-1}.

The crystal structures of complexes **I**–**III** were determined by XRD. The molecular structures of coordination compounds **I**–**III** are shown in Figs. 1–3, respectively. Selected geometric parameters of the coordination spheres of the compounds are given in Table 2.

The nickel ion exists completely in the nitrogen donor environment in all compounds. The coordination polyhedron of the nickel ion in complexes **I**–**III** consists of four nitrogen atoms lying in the pseudo-equatorial plane and two nitrogen atoms of the NCS^- anions occupying the axial positions.

The shortest coordination bonds of the Ni ion are formed with the axial NCS^- ligands. The Ni–N bond lengths in the pseudo-equatorial plane differ significantly, and the distances metal–nitrogen atom of the heterocyclic fragment (Ni–N_{het}) are by ~0.2 Å longer than the distances metal–nitrogen atom of the diacetyl fragment (Ni–N_{diac}), which is due to specific features of the organic ligand structure.

Since three fused five-membered chelate cycles with intracyclic angles at the nickel ion are formed (N(1A)Ni(1)N(3(A)) 75.21(6)°, N(1A)Ni(1)N(1) 75.52(6)° in **I**; N(1)NiN(3) 74.65(5)°, N(1)NiN(4) 75.16(6)°; N(4)NiN(6) 74.80(5)° in **II**; and N(5)Ni(1)N(3) 74.08(8)°, N(5)Ni(1)N(6) 75.68(8), N(6)Ni(1)N(4) 72.77(8)° in **III**) upon the coordination of the Ni ion, the extracyclic angle in the equatorial plane turns out to be significant: N(3A)Ni(1)N(3) 134.23(7)° in **I**, N(3)NiN(6) 135.62(5)° in **II**, and N(3)Ni(1)N(4) 137.44(7)° in **III**. As a result, the deviation of the angle between the nitrogen atoms of the axially coordinated NSC anions ($N_{NCS1}NiN_{NCS2}$) from 180° is observed: N(4)Ni(1)N(4(A)) 169.91(8)° in **I**, N(7)Ni(8)N 166.09(6)° in **II**, and N(1)Ni(1)N(2) 163.59(9)° in **III**. The positions of the nitrogen donor atoms in the pseudo-equatorial plane are characterized by a substantial trapezium-shaped distortion.

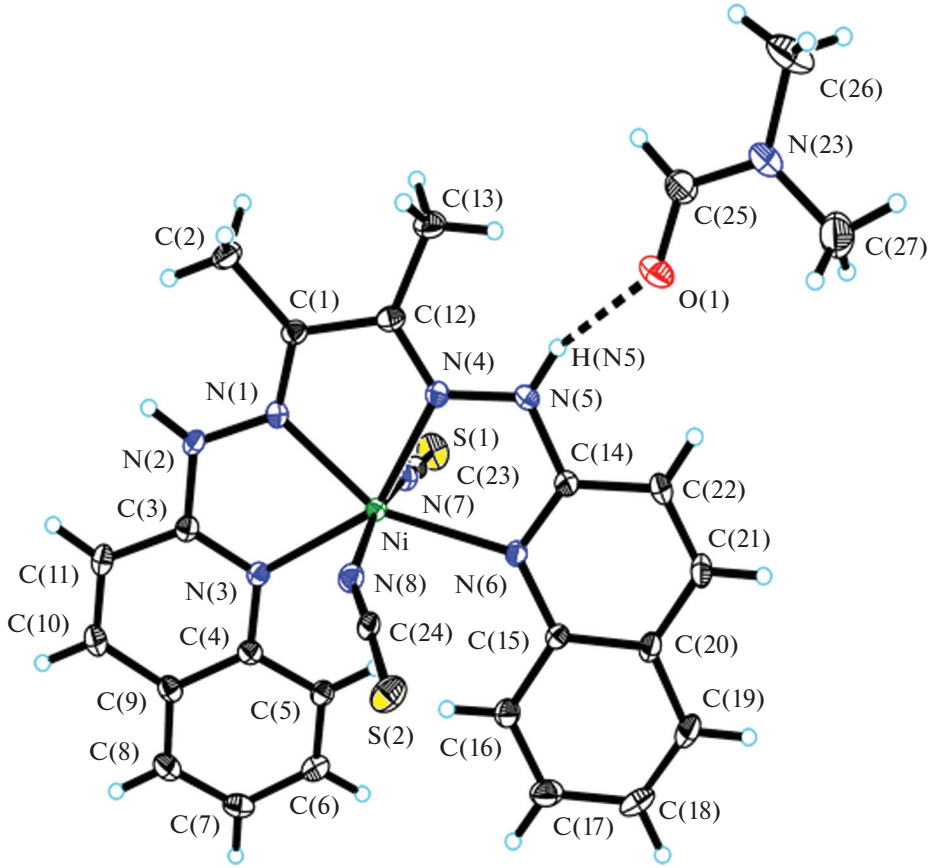

Fig. 2. Molecular structure of complex **II**.

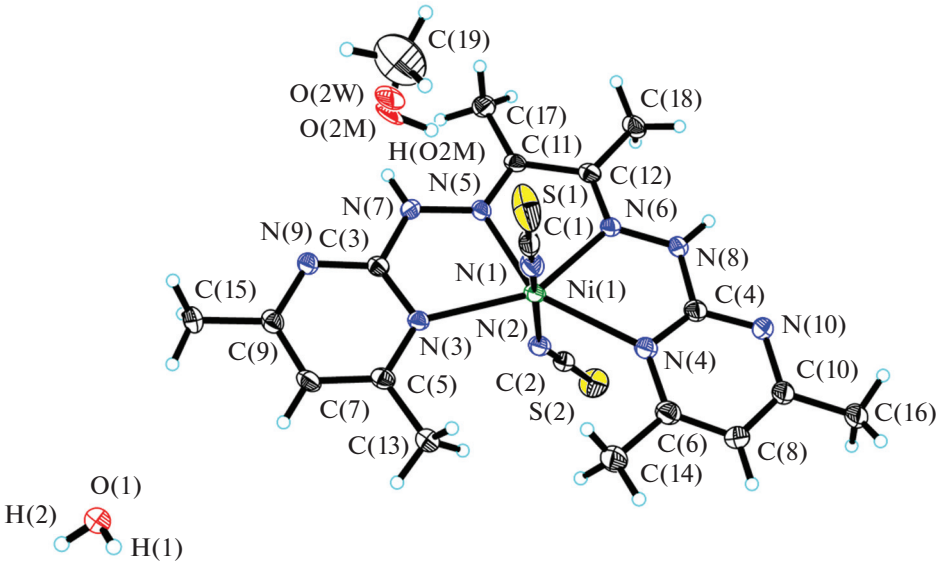

Fig. 3. Molecular structure of complex **III**.

Table 2. Selected geometric parameters of the coordination sphere of the nickel ion in complexes **I**–**III**

Bond	**I**	**II**	**III**
	d, Å		
$Ni–N_{NCS1}$	2.021(2)	2.0155(15)	1.991(2)
$Ni–N_{NCS2}$	2.021(2)	2.0338(15)	2.012(2)
$Ni–N_{het}$	2.2381(16)	2.2500(14)	2.271(2)
$Ni–N_{het}$	2.2381(16)	2.2454(14)	2.2454(14)
$Ni–N_{diac}$	2.0374(17)	2.0498(14)	2.039(2)
$Ni–N_{diac}$	2.0374(17)	2.0494(14)	2.071(2)
Angle	ω, deg		
$N_{NCS1}NiN_{NCS2}$	169.91(8)	166.09(6)	163.59(9)
Intracyclic chelate angles at Ni ion	75.21(6)	74.65(5)	74.08(8)
N(1A)Ni(1)N(1)	75.52(6)	75.16(6)	75.68(8)
	75.21(6)	74.80(5)	72.77(8)
Extracyclic angle at Ni ion	134.23(7)	135.62(5)	137.44(7)

An analysis of the coordination environment using the continuous symmetry measure calculated by the SHAPE 2.1 program [41] in complexes **I**–**III** showed that the hexacoordinated environment of the central Ni^{2+} ion was distorted to a significant extent compared to both the ideal octahedral and trigonal prismatic structures (for the ideal polyhedron structure, the corresponding indicator should be zero). The geometric parameters of the deviation for various probable coordination geometries with six coordination numbers around the Ni center (OC-6* is octahedron (Oh), TPR-6** is trigonal prism (D3h)) are shown below.

I		**II**		**III**	
OC-6*	TPR-6**	OC-6	TPR-6	OC-6	TPR-6
5.514	7.743	6.172	7.291	7.158	7.354

The detailed structure of the coordination polyhedron of the Ni(II) ion in complexes **I**–**III** presented in Fig. 4 clearly shows strong deviations of the

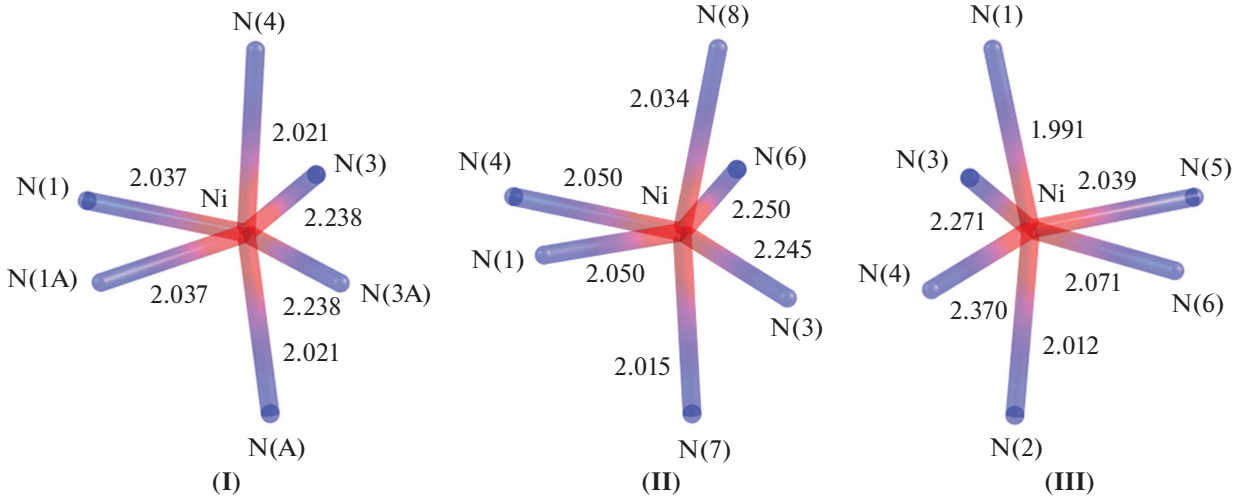

Fig. 4. Polyhedra of compounds **I**–**III**.

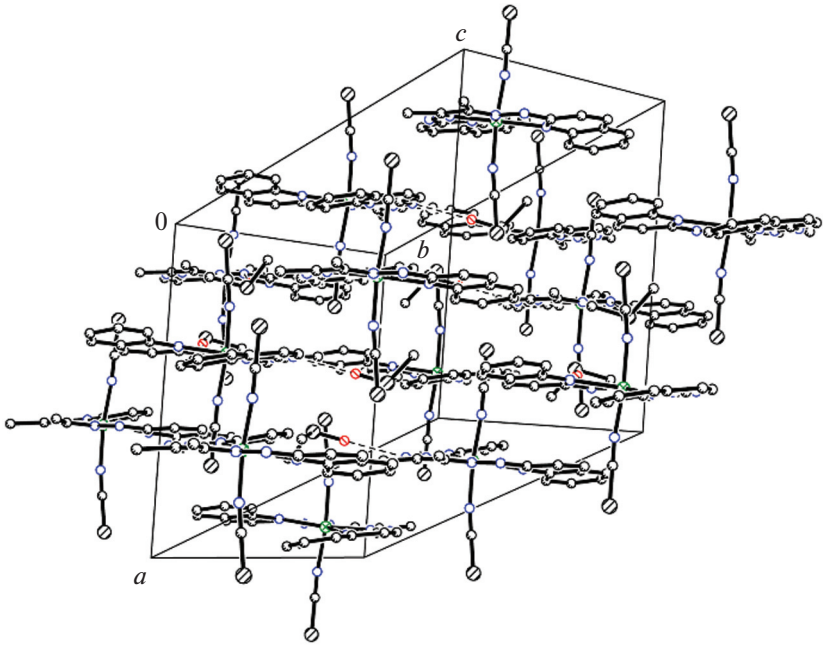

Fig. 5. Fragment of the crystal packing of complex **I** (without hydrogen atoms).

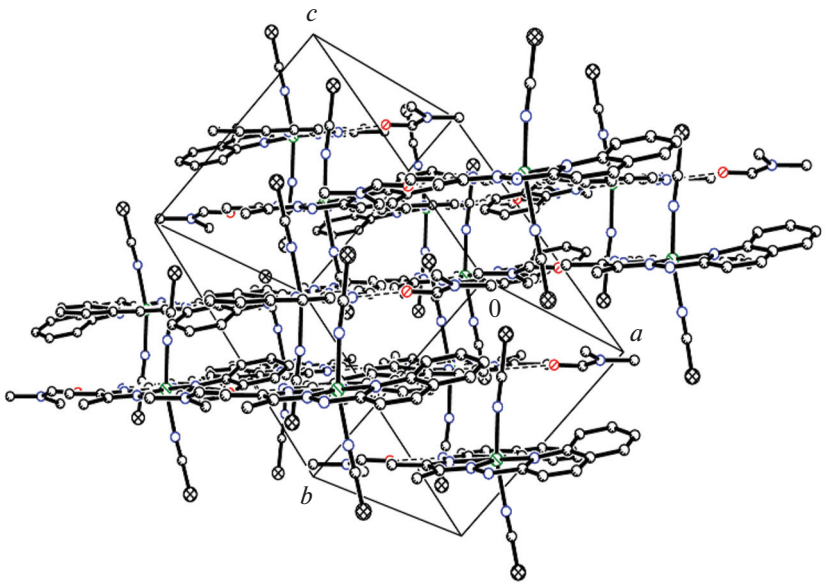

Fig. 6. Fragment of the crystal packing of complex **II** (without hydrogen atoms).

N(4)NiN(4A) angle in **I**, N(7)NiN(8) in **II**, and N(1)NiN(2) in **III** from linearity and the distinction of the geometry of the equatorial plane N(1)N(3)N(1A)N(3A) in **I**, N(1)N(3)N(4)N(6) in **II**, and N(3)N(4)N(5)N(6) in **III** from an ideal square.

The packings of molecules in the crystalline lattice of compounds **I**–**III** is layered as shown in Figs. 5–7, respectively.

The shortest distance between the nickel atoms is as follows: 8.575(3) Å in **I** (the longest one among compounds **I**–**III**), 6.603(3) Å in **II**, and 7.873(3) Å in **III**. In the crystal structure of complex **I**, the oxygen atom of the solvate DMSO molecule forms a weak contact with the hydrogen atom at the N(2) nitrogen atom with the following parameters: O(1A)...N(2) 2.731, O(1A)...H(N2) 1.94(2) Å, O(1A)H(N2)N(2)

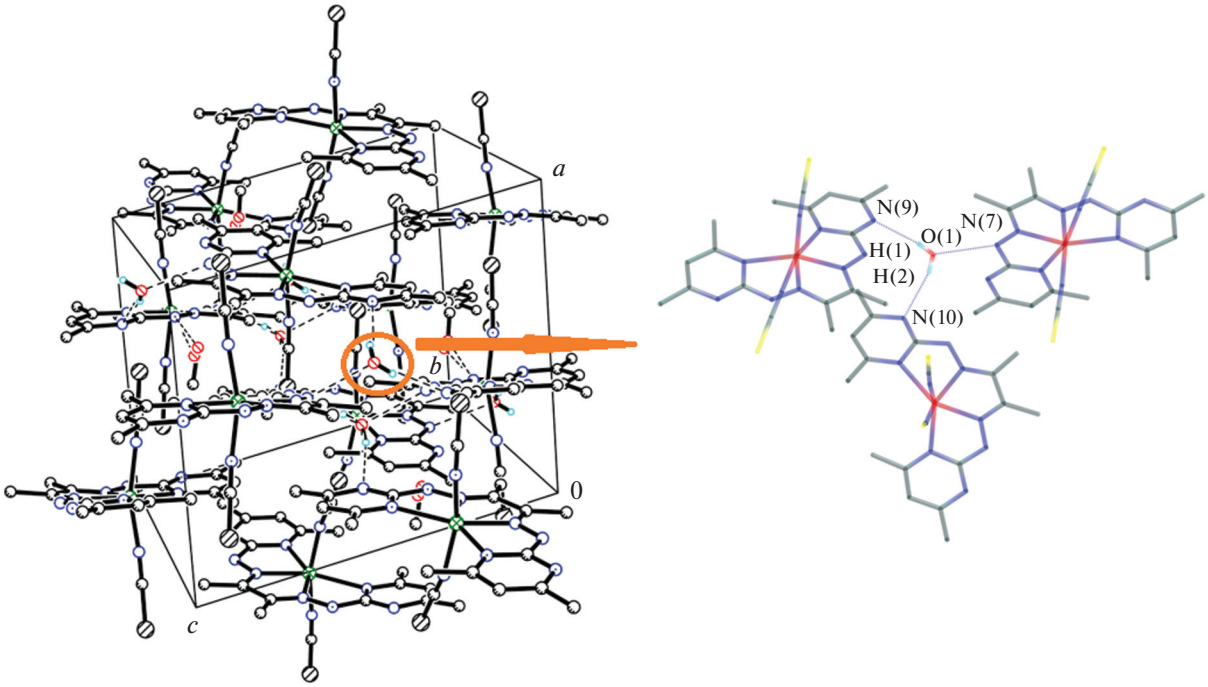

Fig. 7. (a) Fragment of the crystal packing of complex **III** (dashed lines show intermolecular hydrogen bonds formed by the molecule of water of crystallization) and (b) intermolecular hydrogen bonds between the water molecule and molecules of complex **III**.

153.4(7)° O(1B)...N(2) 2.700(3), O(1B)...H(N2) 1.86(1) Å, and O(1B)H(N2)N(2) 165.3(6)°.

In the crystal structure of complex **II**, the solvate molecule of *N*,*N*-dimethylformamide is involved in the formation of an intermolecular hydrogen bond of the N–H...O type (Fig. 6) with the following parameters: O(1)...N(5) 2.739(4), O(1)...H(N5) 1.92(2) Å, and O(1)H(N5)N(5) 158.2(6)°.

In the structure of complex **III**, both hydrogen atoms of the molecules of water of crystallization (H(1)H(2)O(1)) are involved in the formation of two intermolecular hydrogen bonds of the O–H...N type with the parameters H(1)...N(9) 2.15(1), O(1)...N(9) 2.944(3) Å, O(1)H(1)N(9) 172.2(5)° {1/2 + *x*, 1/2 – *y*, 1/2 + *z*} and H(2)...N(10) 2.22(2), O(1)...N(10) 2.922(3) Å, O(1)H(2)N(10) 162.1(6)° {*x*, 1 + *y*, *z*} and one intermolecular hydrogen bonds of the N(7)H...O(1)N(7) type {–1/2 – *x*, 1/2 + *y*, 3/2 – *z*} equal to 2.759(3) Å (Fig. 7).

At room temperature the product of the molar magnetic susceptibility by temperature ($\chi_M T$) is about 1.21 cm^3 K mol^{-1} (Fig. 8), which is somewhat higher than the spin-only value (~1.00 cm^3 K mol^{-1}) for $S = 1$ and $g = 2$. On cooling to 20 K, $\chi_M T$ decreases sharply and reaches ≈0.38 cm^3 K mol^{-1} at 2 K. This low-temperature decrease in $\chi_M T$ can be explained by the presence of magnetic anisotropy related to the zero-field splitting.

The following anisotropic spin-Hamiltonian (1) was used to describe the magnetic properties of complex **III** in a permanent magnetic field:

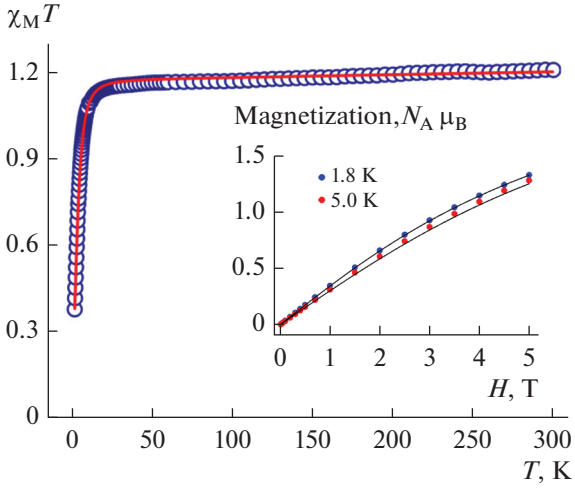

Fig. 8. Temperature dependence of $\chi_M T$ for compound **III** measured at $H = 0.1$ T (hollow circles). Inset: the magnetization from the field for compound **I** measured at $T = 1.8$ and 5 K. The theoretical curves (solid lines) were calculated with the following parameters: $E = 0.08$ cm^{-1} $g_X = g_Y = 2.20$, $g_Z = 2.09$, $\chi_{TIP} = 10 \times 10^{-4}$ cm^3 K mol^{-1}.

Table 3. Calculated (NEVPT2) (for **I**–**III**) and experimental (for **III**) components of the *g* and *D* tensor

Parameter	I	II	III	
	NEVPT2	NEVPT2	Exp.	NEVPT2
D, cm^{-1}	+9.87	+11.6	+8.79	+11.5
E, cm^{-1}	1.38	1.42	0.08	1.68
g_X	2.275	2.293	2.20	2.306
g_Y	2.243	2.259	2.20	2.272
g_Z	2.188	2.195	2.09	2.206

$$\hat{H} = D\left[\hat{S}_Z^2 - \frac{1}{3}S(S+1)\right] + E\left[\hat{S}_X^2 - \hat{S}_Y^2\right] + \mu_B\left(B_X g_X \hat{S}_X + B_Y g_Y \hat{S}_Y + B_Z g_Z \hat{S}_Z\right), \quad (1)$$

where $S = 1$ is the spin of the Ni^{2+} ion; D and E are the axial and orthorhombic splitting parameters in the zero field, respectively; and $g_\alpha\,(\alpha = X, Y, Z)$ are the *g*-tensor components. The set of optimum parameters is as follows: $|D| = 8.79\ cm^{-1}$, $E = 0.08\ cm^{-1}$, $g_Z = 2.09$, $g_X = g_Y = 2.20$, and $\chi_{TIP} = 10 \times 10^{-4}\ cm^3\ K\ mol^{-1}$ (TIP-temperature-independent paramagnetism).

The absolute value of the axial splitting parameter in the zero field was obtained. The magnetization as a function of the magnetic field measured at $T = 1.8$ and 5 K is shown in Fig. 8 (inset).

The results of the magnetochemical study showed no slow magnetization relaxation for complex **III** in either applied, or zero field.

The *g*- and *D*-tensor components were calculated in terms of the multideterminant CASSCF + NEVPT2 wavefunction in the QDPT approximation in order to determine the axial splitting parameter in the zero field of compounds **I**–**III**. The calculation results are presented in Table 3.

Table 4. Splitting of the *d*-AO (cm^{-1}) calculated in the framework of the AILFT for compounds **I**–**III** (NEVPT2)

State	I	II	III
d_{xy}	0.0	0.0	0.0
$d_{xz} + d_{yz}$	463	356	693
$d_{xz} - d_{yz}$	1409	1341	1371
d_{x2-y2}	6184	6856	6460
d_{z2}	9769	10636	10407

Compound **III** demonstrates a good convergence between the theoretical parameter D_{calc} and D_{exp} obtained by the approximation of the results of magnetic measurements. The calculation indicates three-axis magnetic anisotropy close to the light magnetization plane ($g_X \approx g_Y > g_Z$) with the positive parameter $D > 0$ for all compounds.

It is known [10, 42, 43] that the sign and value of the D_{kl} ($k, l = x, y, z$) component of the magnetic anisotropy tensor is determined by the sum of contributions from one-electron excitations with the retention of spin multiplicity as follows (excitation contributions with a change in the spin multiplicity are determined by additional terms):

$$D_{kl} = -\frac{\zeta_{eff}^2}{4S^2}\sum_{i,p}\frac{\langle\psi_i|\hat{l}_k|\psi_p\rangle\langle\psi_p|\hat{l}_l|\psi_i\rangle}{\varepsilon_p - \varepsilon_i}, \quad (2)$$

where S is the total spin of the ground state, ζ_{eff}^2 is the effective constant of the spin-orbital interaction of the metal ion, $\{\psi\}$ is the multiplicity of molecular orbitals with the energy $\{\varepsilon\}$, and indices i and p correspond to the doubly and singly occupied MOs in the ground state, respectively. The operator $\hat{l}_k$ is the kth component of the orbital angular moment operator ($k, l = x, y, z$).

For the D_{zz} component, the contribution is inversely proportional to the transition energy (transitions between the orbitals with the lowest difference in energies provide the highest (by modulus) contribution) and the sign depends on the nature of the orbitals determining the transition: if both orbitals are characterized by the same (by modulus) quantum number of the orbital moment projection m_l (these are pairs d_{xz}, d_{yz} with $m_l = \pm 1$ and d_{xy}, d_{x2-y2} with $m_l = \pm 2$), then the contribution is negative; if the quantum numbers are different, then the sign of the contribution is positive.

The general scheme of splitting of orbitals of the *d* sublevel of the Ni^{2+} ion calculated in terms of the AILFT approximation is the same for compounds **I**–**III** (Fig. 9 shows the splitting scheme for complex **III** as an example) and corresponds to the axially con-

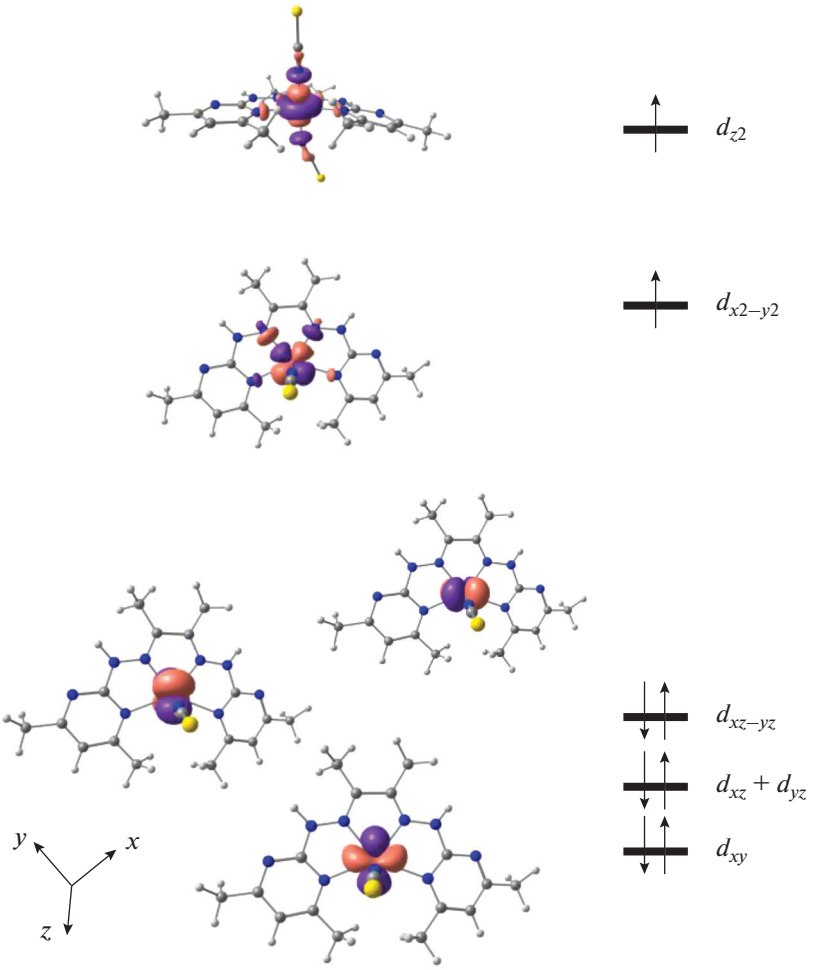

Fig. 9. Splitting of the *d*-AO of the nickel ion in complex **III** (calculated according to the AILFT). The axes of coordinates are oriented as follows: the *z* axis is perpendicular to the molecule plane, and the *x* and *y* axes are directed to the nitrogen atoms.

tracted octahedron, which coincides with the XRD data according to the which the Ni–NCS distances are shortest.

The calculated relative energies of the corresponding orbitals for compounds **I**–**III** are listed in Table 4.

The lowest in energy is the d_{xy} orbital, whose maxima are directed to the space between the nitrogen donor atoms. Two combinations of *d*-AOs lie higher in energy: $d_{xz} + d_{yz}$ and $d_{xz} - d_{yz}$. The d_{z2} orbital is most destabilized due to its significant antibonding interaction with the group σ orbitals of the axially coordinated NCS^- anions. The d_{x2-y2} orbital is stabilized to a significantly lower extent owing to the trapezium arrangement of the donor nitrogen atoms in the equatorial plane, which results in the elongation of the Ni–N distance in the heterocyclic fragment and, hence, in a decrease in the strength of the ligand field.

Evidently, excitations with the lowest energy would correspond to the electron transition from the lowest doubly occupied orbitals to the lowest of the singly occupied orbitals (d_{x2-y2}). Two transitions ($d_{xz} + d_{yz} \rightarrow$

Table 5. Highest (by modulus) individual contributions (cm^{-1}) of electron excited states to the *D* parameter (NEVPT2)

Multiplicity of excited state	Number of excited state	I	II	III
3	1	25.02	26.54	27.50
3	2	21.79	23.02	19.81
3	3	–34.46	–35.66	–33.27
1	1	–7.77	–7.90	–7.89
1	2	–6.68	–6.74	–6.59
1	3	13.01	13.27	13.37

d_{x2-y2} and $d_{xz} - d_{yz} \rightarrow d_{x2-y2}$) will provide the positive contribution, and one transition ($d_{xy} \rightarrow d_{x2-y2}$) provides the negative contribution. At approximately equal transition energies (and, correspondingly, equal contributions), the total value should be positive.

The performed analysis is completely confirmed by the calculation results of individual contributions of the excitations to the *D* parameter, the highest (by modulus) of which are given in Table 5.

The first two triplet excitations provide the positive contributions and the third excitation provides the negative contribution, which totally gives the positive *D*. The contributions from transitions to the excited singlet states are substantially lower by modulus and approximately compensate each other without affecting the sign and value of the *D* parameter.

Thus, the coordination Ni(II) compounds with the tetradentate ligands derived from the products of the condensation of diacetyl with 2-hydrazinoquinoline (L^1) and 2-hydrazino-4,6-dimethylpyrimidine (L^2) were synthesized. The molecular and crystal structures of compounds $[NiL^1(NCS)_2]\cdot 2DMSO$ (**I**), $[NiL^1(NCS)_2]\cdot DMF$ (**II**), and $[NiL^2(NCS)_2]\cdot CH_3OH\cdot 3H_2O$ (**III**) were determined by XRD in combination with IR spectroscopy. The complexes were shown to be characterized by three-axis magnetic anisotropy close to the light magnetization plane with the positive axial parameter of magnetic anisotropy *D*. It has been found for compound **III** as an example that similar complexes demonstrate slow magnetic magnetization relaxation.

FUNDING

XRD analysis of compounds **I**–**III** was carried out at the Federal Research Center of Problems of Chemical Physics and Medicinal Chemistry (Russian Academy of Sciences) in the framework of state assignment no. 124013100858-3.

CONFLICT OF INTEREST

The authors of this work declare that they have no conflicts of interest.

REFERENCES

1. Troiani, F. and Affronte, M., *Chem. Soc. Rev.*, 2011, vol. 40, no. 6, p. 3119.
2. Stamp, P.C. and Gaita-Arino, A., *J. Mater. Chem.*, 2009, vol. 19, no. 12, p. 1718.
3. Timco, G.A., Faust, T.B., Tuna, F., et al., *Chem. Soc. Rev.*, 2011, vol. 40, no. 6, p. 3067.
4. Sanvito, S., *Chem. Soc. Rev.*, 2011, vol. 40, no. 6, p. 3336.
5. Novikov, V.V. and Nelyubina, Yu.V., *Russ. Chem. Rev.*, 2021, vol. 90, no. 10, p. 1330.
6. Neese, F. and Pantazisa, D.A., *Faraday Discuss.*, 2011, vol. 148, p. 229.
7. Boca, R., *Coord. Chem. Rev.*, 2004, vol. 248, nos. 9–10, p. 757.
8. Ganyushin, D. and Neese, F., *J. Chem. Phys.*, 2006, vol. 125, no. 2, p. 024103.
9. Cirera, J., Ruiz, E., Alvarez, S., et al., *Chem.-Eur. J.*, 2009, vol. 15, no. 16, p. 4078.
10. Sarkar, A., Dey, S., and Rajaraman, G., *Chem.-Eur. J.*, 2020, vol. 26, no. 62, p. 14036.
11. Craig, G.A. and Murrie, M., *Chem. Soc. Rev.*, 2015, no. 44, p. 2135.
12. Bar, A.K., Pichon, C., and Sutter, J.-P., *Coord. Chem. Rev.*, 2016, vol. 308, p. 346.
13. Tupolova, Y.P., Lebedev, V.E., and Shcherbakov, I.N., *New J. Chem.*, 2023, vol. 47, no. 22, p. 10484.
14. Tupolova, Y.P., Korchagin, D.V., Andreeva, A.S., et al., *Magnetochemistry*, 2022, vol. 8, no. 11, p. 153.
15. Popov, L.D., Morozov, A.N., Shcherbakov, I.N., et al., *Russ. Chem. Rev.*, 2009, vol. 78, no. 7, p. 643.
16. Nikolaevskaya, E.N., Druzhkov., N.O., Syroeshkin, M.A., et al., *Coord. Chem. Rev.*, 2020, vol. 417, p. 213353.
17. Tupolova, Yu.P., Shcherbakov, I.N., and Korchagin, D.V., et al., *J. Phys. Chem. C*, 2020, vol. 124, no. 47, p. 25957.
18. Tupolova, Y.P., Lebedev, V.E., Korchagin, D.V., et al., *New J. Chem.*, 2023, vol. 47, no. 22, p. 10884.
19. Tupolova, Y.P., Shcherbakov, I.N., Popov, L.D., et al., *Dalton Trans.*, 2019, vol. 48, p. 6960.
20. Dziomko, V.M., Krasavin, I.A., and Miroshkina, N.I., *Metody Poluch. Khim. Reakt. Prep.*, 1965, no. 12, p. 50.
21. Kosolapoff, G.M. and Roy, C.H., *Org. Chem.*, 1961, vol. 26, p. 1895.
22. Tupolova, Y.P., Korchagin, D.V., Lebedev, V.E., et al., *Russ. J. Coord. Chem.*, 2022, vol. 48, p. 362.
23. *CrysAlisPro. Version 1.171.38.41. Rigaku Oxford Diffraction*, 2015. https://www.rigaku.com/en/products/smc/crysalis.
24. *SHELXTL. Version 6.14*, Madison: Bruker AXS, 2000.
25. Roos, B.O., Taylor, P.R., and Sigbahn, P.E.M., *Chem. Phys.*, 1980, vol. 48, no. 2, p. 157.
26. Per, S., Anders, H., Björn, R., and Bernard, L., *Phys. Scr.*, 1980, vol. 21, nos. 3–4, p. 323.
27. Siegbahn, P.E.M., Almlöf, J., Heiberg, A., et al., *J. Chem. Phys.*, 1981, vol. 74, no. 4, p. 2384.
28. Angeli, C., Cimiraglia, R., Evangelisti, S., et al., J. *Chem. Phys.*, 2001, vol. 114, no. 23, p. 10252.
29. Angeli, C., Cimiraglia, R., and Malrieu, J.-P., *Chem. Phys. Lett.*, 2001, vol. 350, no. 3, p. 297.
30. Angeli, C. and Cimiraglia, R., *Theor. Chem. Acc.*, 2002, vol. 107, no. 5, p. 313.
31. Angeli, C., Cimiraglia, R., and Malrieu, J.-P., *J. Chem. Phys.*, 2002, vol. 117, no. 20, p. 9138.

32. Hess, B.A., *Phys. Rev. A*: *At., Mol. Opt. Phys.*, 1986, no. 6, p. 3742.
33. Pantazis, D.A., Chen, X.Y., Landis, C.R., et al., *J. Chem. Theory Comput*., 2008, vol. 4, p. 908.
34. Schafer, A., Huber, C., and Ahlrichs, R., *J. Chem. Phys.*, 1994, vol. 100, no. 8, p. 5829.
35. Schafer, A., Horn, H., and Ahlrichs, R., *J. Chem. Phys.*, 1992, vol. 97, no. 4, p. 2571.
36. Weigend, F. and Ahlrichs, R., *Phys. Chem. Chem. Phys.*, 2005, vol. 7, no. 18, p. 3297.
37. Neese, F., *J. Comput. Chem.*, 2003, vol. 24, no. 14, p. 1740.
38. Neese, F., *WIREs Comput. Mol. Sci.*, 2018, vol. 8, no. 1, p. e1327.
39. Atanasov, M., Ganyushin, D., Sivalingam, K., et al., in *Molecular Electronic Structures of Transition Metal Complexes II*, Mingos, D.M.P., Day, P., Dahl, J.P, Eds., Berlin, Heidelberg: Springer, 2012, p. 149.
40. Singh, S.K., Eng, J., Atanasov, M., et al., *Coord. Chem. Rev.*, 2017, vol. 344, p. 2.
41. Alvarez, S., Alemany, P., and Casanova, D., J, et al., *Coord. Chem. Rev.*, 2005, vol. 249, p. 1693.
42. Gómez-Coca, S., Cremades, E., Aliaga-Alcalde, N., et al., *J. Am. Chem. Soc.*, 2013, vol. 135, no. 18, p. 7010.
43. Gómez-Coca, S., Aravena, D., Morales, R., et al., *Coord. Chem. Rev.*, 2015, vols. 289–290, p. 379.

Translated by E. Yablonskaya